



SUBJECT AREAS:

METAMATERIALS

NANOWIRES

SUB-WAVELENGTH OPTICS

NANOPHOTONICS AND  
PLASMONICS

# Ultra low-loss, isotropic optical negative-index metamaterial based on hybrid metal-semiconductor nanowires

R. Paniagua-Domínguez, D. R. Abujetas &amp; J. A. Sánchez-Gil

Instituto de Estructura de la Materia, Consejo Superior de Investigaciones Científicas, Serrano 121, 28006 Madrid, Spain.

Received  
1 February 2013Accepted  
6 March 2013Published  
21 March 2013Correspondence and  
requests for materials  
should be addressed to  
J.A.S.-G. (j.sanchez@  
csic.es)

Recently, many fascinating properties predicted for metamaterials (negative refraction, superlensing, electromagnetic cloaking,...) were experimentally demonstrated. Unfortunately, the best achievements have no direct translation to the optical domain, without being burdened by technological and conceptual difficulties. Of particular importance within the realm of optical negative-index metamaterials (NIM), is the issue of simultaneously achieving strong electric and magnetic responses and low associated losses. Here, hybrid metal-semiconductor nanowires are proposed as building blocks of optical NIMs. The metamaterial thus obtained, highly isotropic in the plane normal to the nanowires, presents a negative index of refraction in the near-infrared, with values of the real part well below  $-1$ , and extremely low losses (an order of magnitude better than present optical NIMs). Tunability of the system allows to select the operating range in the whole telecom spectrum. The design is proven in configurations such as prisms and slabs, directly observing negative refraction.

The so called metamaterials are artificial materials in which the effective medium properties, usually exotic and not naturally attainable, depend on the geometry of their basic constituents, rather than on their chemical composition<sup>1,2</sup>. Ranging from sub-diffraction resolution<sup>3,4</sup> or spontaneous emission<sup>5</sup> to extreme control over the flow of light<sup>6,7</sup>, many exciting and unexpected phenomena have been achieved or predicted for this new kind of materials. Although originally developed in electromagnetics, many of the ideas developed in this field have been successively extended or adapted to other ondulatory phenomena, such as acoustics, making it one of the most active in the engineering and physical sciences in the past few years.

Still, however, there are many open challenges in the field. Among them, the realization of a bulk isotropic negative index metamaterial (NIM), with negative refraction and low losses in the optical domain<sup>8,9</sup>. In general terms, the major issue when trying to achieve such a goal is obtaining a strong diamagnetic response of the constituents, enough to lead to an effective negative permeability. Probably as a consequence of the success of the original designs operating in the microwave regime, many efforts were made to adapt them to increasingly higher frequencies, mainly by miniaturization<sup>8,9</sup>. Apart from some inherited from the original designs, such as anisotropy, many drawbacks were found in doing so, mainly related to the different behaviour of metals at optical frequencies, such as saturation of the magnetic response<sup>10</sup> or high losses associated to ohmic currents. As a consequence, completely different strategies were studied to obtain artificial magnetism<sup>11,12</sup>, as those based in displacement currents appearing in nanoparticle clusters due to coupling between structures<sup>13</sup>. However, some of the most successful were those which attempted to obtain it from natural magnetic resonant modes in high permittivity dielectrics, leading to low-loss magnetic materials<sup>14-18</sup>. Secondary structures or particular arrangements were needed to provide the additional electrical response, necessary to obtain doubly negative index of refraction<sup>19-21</sup>. Thus far, the maximum theoretical figure of merit (f.o.m. =  $-Re(n_{eff})/Im(n_{eff})$ ) reported is of the order of f.o.m.  $\sim 25^{22-24}$  for metamaterials based on canonical fishnet designs; their dimensions, however, are in the very limit of validity of the effective medium description, and isotropy was not proven (see<sup>25</sup> for a review on this topic).

In this work, we propose a structure that, combining electric and magnetic responses, can be used as the basic building block for extremely low-loss (f.o.m.  $\sim 200$ ) isotropic two-dimensional metamaterials in the near-infrared, with simultaneously negative permittivity ( $\epsilon$ ) and permeability ( $\mu$ ) at optical frequencies. Such structure is a core-shell nanowire (NW) of circular cross section. Noble metals such as silver or gold can be employed to build the core, and high permittivity semiconductors, such as silicon or germanium, to build the shell. Artificial magnetism of the effective medium is achieved by exciting the lowest order Mie-like magnetic resonance in



the wires. We show that it is possible to tune the geometrical parameters of the system to make this resonance spectrally overlap with the lowest electric, dipole-like, one, in turn a localized surface plasmon resonance (LSPR) excitation in the metallic core. Polarization of the incident wave with the magnetic field along the axis of the wires (TE-polarization) will generate the desired responses.

## Results

**Electric and magnetic resonances of single hybrid nanowires.** The optical properties of coated cylinders under plane wave illumination can, indeed, be analytically studied<sup>26</sup>. Under TE polarized light, the scattering and extinction efficiencies of these particles can be written as sums over different coefficients:

$$Q_{sca} = \frac{2}{x} \left( |a_0|^2 + 2 \sum_{j=1}^{\infty} |a_j|^2 \right) \quad (1)$$

$$Q_{ext} = \frac{2}{x} \operatorname{Re} \left( a_0 + 2 \sum_{j=1}^{\infty} a_j \right) \quad (2)$$

which can be then assigned a certain multipolar character, either magnetic or electric. Although the expressions are similar to those of a solid cylinder (i.e., without coating), the  $a_j$  coefficients contain information about both the core and the shell (see Supplementary Information, Section 1). With this given polarization, the first zero-order coefficient,  $a_0$ , has magnetic character, while the second coefficient,  $a_1$ , can be identified as the electric dipolar contribution in the 2D plane perpendicular to the cylinder axis.

We can realize that this is the case if we study the optical properties of a pure silicon (Si) cylinder. Incidentally, Silicon spheres<sup>18</sup> have attracted the interest of the community, because of their potential use in metamaterials and interesting radiative properties. In Fig. 1 we have plotted the scattering efficiency of a solid Si cylinder of radius  $R = 170$  nm under normal incidence of a TE-polarized plane wave. It can be immediately realized that the optical properties are quite similar to those of a pure Si sphere<sup>18</sup>, although the correspondence between Mie coefficients and electric and magnetic multipolar terms is not straightforward for cylinders. Thus, we need to identify the character of the  $a_0$  and  $a_1$  coefficients. To this end, we plot the total

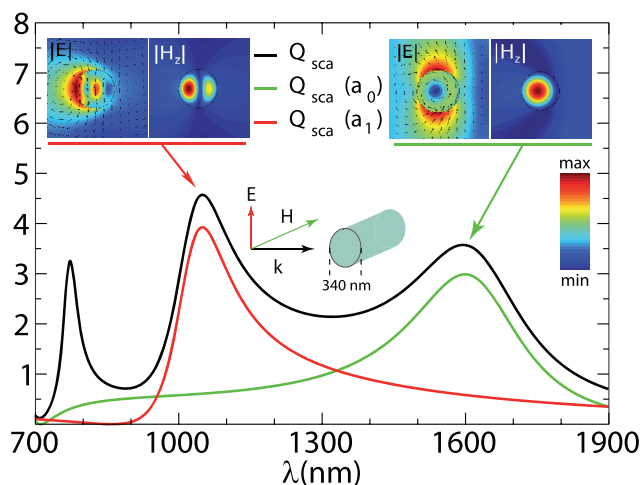


**Figure 1 | Optical properties of an infinite silicon nanocylinder.** Scattering efficiency (black curve) of a silicon cylinder with radius  $R = 170$  nm under TE-polarized plane wave incidence. Contributions of the two first terms in the expansion of the field are also shown. Depicted in the insets are the maps of the near electric field (left), and out-of-plane component of the magnetic field (right) at the magnetic (green,  $\lambda_0 = 1605$  nm) and electric (red,  $\lambda_0 = 1050$  nm) resonances. The TE-polarized plane wave impinges from the right hand side.

electric field and the out-of-plane component (only non-zero) of the magnetic field in the insets of Fig. 1 for the first two resonances. Similar to the case of a sphere, the magnetic resonance is the one excited at lower frequencies (green curve), thus corresponding to the  $a_0$  coefficient. The strong circulation of the electric field is a clear signature of the magnetic character of the resonance. On the other hand, the subsequent higher-energy resonance reveals the dipolar electric character of the  $a_1$  resonance.

Combining a dielectric shell, which exhibits magnetic properties similar to those of solid cylinders, with a plasmonic core, will provide the additional electric resonance necessary to obtain a doubly resonant structure suitable as a NIM building block (meta-atom). In order to make both resonances spectrally overlap, tuning of the geometrical parameters of the structure is needed. This approach has been successfully employed in the case of a core-shell sphere<sup>27</sup>, but it has to be proven for a core-shell cylinder due to the different behaviour of its magnetic resonance. In Fig. 2a, we have plotted the magnetic and electric contributions to the scattering, together with the total efficiency, for core-shell NWs of outer radius  $R_{out} = 170$  nm as a function of the wavelength of incidence and inner radius ( $R_{int}$ ).

The materials used are silver (Ag) for the core, and Si for the shell. The electric and magnetic responses spectrally overlap over a relatively wide range,  $\lambda_0 \in (1100, 1500)$  nm, for  $R_{int}$  values between 60 and 100 nm. This makes the core-shell nanowire design particularly robust against possible fabrication defects. Notice that, in the limit of  $R_{int} \rightarrow 0$ , we recover those values of the pure Si cylinder. Although essentially similar, both resonances redshift in the case of Ge coating for the same fixed  $R_{out}$  value, due to the slightly higher index of refraction of this material. The study of this case can be found in Section 2 of the Supplementary Information (see Supplementary Figure 1).

Let us choose a particular value of  $R_{int}$ , namely  $R_{int} = 80$  nm. In Fig. 2b the total scattering efficiency is plotted, together with the magnetic ( $a_0$ ) and electric ( $a_1$ ) contributions. These two contributions are totally dominant in the frequency range in which both coincide. Moreover, plotting the near-field distributions of both the electric and magnetic fields at the frequency of coincidence of the resonances allows one to identify the electric and magnetic character of the combined resonance. Indeed, a strong rotation of the electric field is observed, together with the signature in the magnetic field of a LSPR excitation in the core of the system (see insets in Fig. 2b).

Metallo-dielectric core-shell NWs are, therefore, doubly resonant structures, having a relatively small electrical size. In the Ag@Si case studied, this electrical size reduces to  $R_{out}/\lambda_{res} \sim 0.13$ . These properties allow one to envisage a possible application as building blocks for NIM at optical frequencies, as their spherical geometry counterparts<sup>27</sup>. Indeed, for compact arrangements, with lattice periods of about the size of the diameter of the wires, the metamaterials thus obtained may be well described as an effective medium (depending also on the absolute values of the effective index of refraction,  $n_{eff}$  achieved). These compact arrangements can actually be employed in realistic designs, if we just impose the structures to be unconnected. This is a necessary requirement in order to keep the magnetic resonance condition of the system unchanged. Coupling between neighbouring particles is small, since most of the electromagnetic energy is localized well inside the shell (see right inset in figure 2). Thus, as will be shown later, no significant coupling occurs in general, even if we bring the structures very close<sup>27</sup>.

**Physical origin of the negative index of refraction. The negative permeability.** Before going into the study of the optical properties of arrangements of these core-shell nanowires, let us show that the doubly resonant character of these core-shell nanostructures can lead, indeed, to an effective negative index of refraction. Contrary to some other metamaterial designs in which the electromagnetic

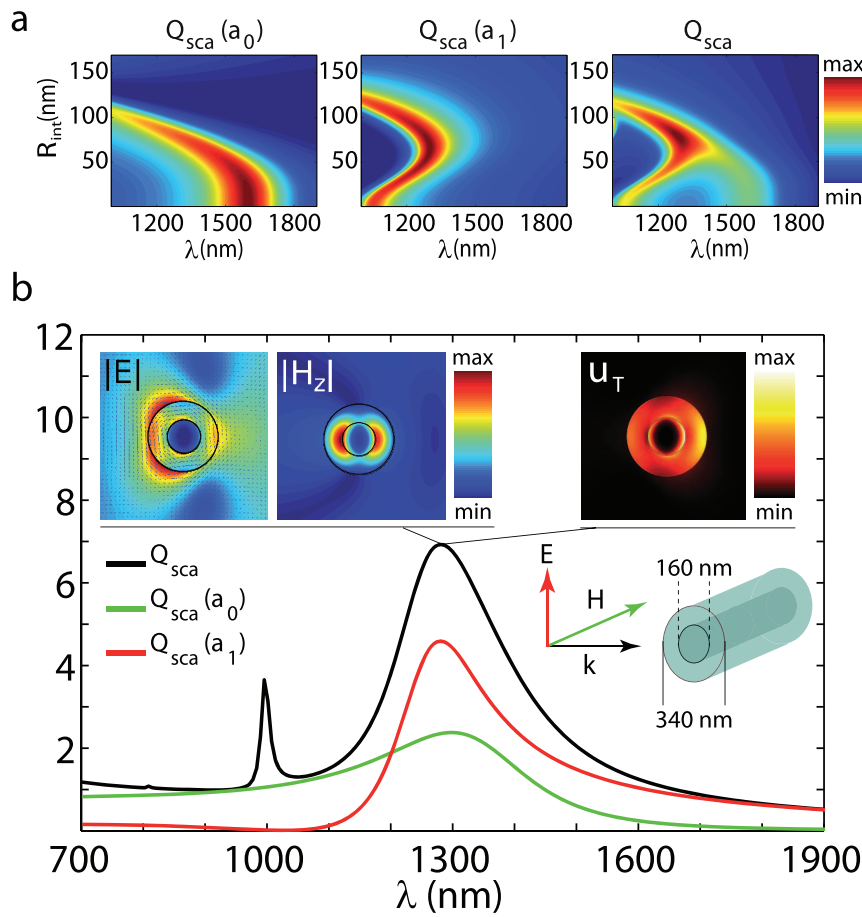


**Figure 2 | Optical properties of an infinite silver-silicon core-shell nanocylinder.** (a) Magnetic (left) and dipolar electric (centre) contributions to the total scattering efficiency (right) of a 170 nm Ag covered with Si (Ag@Si) core-shell nanocylinder as a function of the inner radius,  $R_{\text{int}}$ , and the incident wavelength. (b) Scattering efficiency (black curve) for a Ag@Si core-shell nanowire with external radius  $R_{\text{out}} = 170$  nm and internal radius  $R_{\text{int}} = 80$  nm. Electric (red curve) and magnetic (green curve) contributions are also shown. Depicted in the inset are the maps of the near electric field ( $|E|$ , left), out-of-plane component of the magnetic field ( $|H_z|$ , center) and total electromagnetic energy density ( $u_T$ , right) at the combined resonance, i.e., at  $\lambda_0 = 1298$  nm. The TE-polarized plane wave impinges from the right hand side.

response is such that a wave incident from free space experiences negative refraction in the metamaterial although the phase front always undergoes positive refraction<sup>12</sup>, the design proposed here is such that both the electric and magnetic material parameters are simultaneously negative, leading, as will be shown below, to negative refraction with actual phase reversal.

Being a negative magnetization the key property to access negative permeability once we neglect possible anisotropic effects, it becomes necessary that the basic constituents present a strong negative magnetic moment:

$$\mathbf{m} = \frac{1}{2} \int_V \mathbf{r} \times \mathbf{J}(\mathbf{r}) d\mathbf{r} \quad (3)$$

where  $V$  represents the volume of the particle.

If we assume the whole current to be a polarization current,  $\mathbf{J} \sim (\epsilon - 1)\mathbf{E}$ , the magnetic moment of each core-shell nanowire is simply given by:

$$\mathbf{m} = \frac{-i\omega}{2} \int_V \epsilon_0[\epsilon(\mathbf{r}) - 1](\mathbf{r} \times \mathbf{E}(\mathbf{r})) d\mathbf{r} \quad (4)$$

If we now take into account the translational symmetry of the system along  $z$ , with the polarization current localized in the two-dimensional plane perpendicular to the nanowire's axis, we can define a magnetic moment per unit length, which is necessarily directed along the nanowire's axis  $\hat{\mathbf{m}} = \hat{m}_z \hat{\mathbf{z}}$ , with:

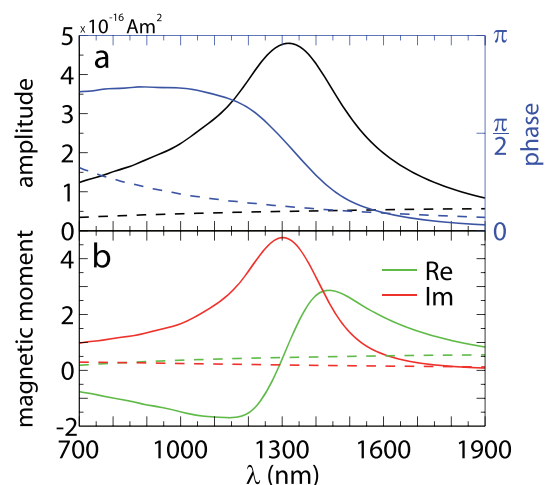


**Figure 3 | Magnetic moment of an infinite silver-silicon core-shell nanocylinder.** (a) The amplitude (black curves) and phase (blue curves), and (b) real (green curves) and imaginary (red curves) parts of the magnetic moment generated on a Ag@Si core-shell nanowire with  $R_{\text{in}} = 80$  nm and  $R_{\text{out}} = 170$  nm under a TE-polarized plane wave incidence are depicted as solid lines. Corresponding dashed lines are the values for a Ag nanocylinder of radius 70 nm embedded in a Si matrix.



$$\tilde{m}_z = \frac{-i\omega}{2} \int_A \epsilon_0[\epsilon(r) - 1](xE_y - yE_x) dA \quad (5)$$

In figure 3a, we have plotted both the amplitude and phase of the magnetic moment generated on a Ag@Si core-shell nanowire with  $R_{in} = 80$  nm and  $R_{out} = 170$  nm under a TE-polarized plane wave incidence. Its resonant behaviour is manifested as an increase of the amplitude and an abrupt change in its phase. This change in the phase makes the real part of the magnetic moment become negative at frequencies above that of the resonance ( $\lambda_0 = 1298$  nm), see figure 3b. It is precisely for this frequency for which the phase acquires the value  $\pi/2$ .

The generation of such strong magnetic moment can also be seen as a consequence of the strong circulation of the electric displacement field in the shell of the system (see inset panel in figure 2b). To prove that this interpretation is correct, the magnetic moment of a pure Ag cylinder of radius 70 nm embedded in a Si matrix has been also computed (dashed lines in figure 3). This system presents a broad electric dipole resonance in its scattering cross section for  $\lambda_0 \sim 1.4$   $\mu\text{m}$ . Nevertheless, the magnetic properties of the system completely disappear, as evidenced through its magnetic moment.

It is easy to envisage that, when enough number of these core-shell nanoparticles are present in a medium, the total magnetization, defined as the magnetic moment per unit volume, can reach negative values, and so can the effective magnetic permeability of the system.

**Optical response of a periodic arrangement of doubly-resonant hybrid nanowires.** Let us now show that it is, actually, possible to obtain a NIM with these nanoparticles. To do so, we arrange the meta-atoms in one of the most common periodic arrangements, namely, a hexagonal lattice. We simulate infinite slabs of different thicknesses to retrieve the effective index of refraction from complex reflection and transmission coefficients<sup>27–29</sup>. Real parts of the effective index of refraction are, moreover, obtained by simply applying Snell's law. This is done under several angles of incidence ( $\theta_i$ ). The retrieved parameters are then tested to fulfil Snell's law also in prism configurations. In the following, it will be demonstrated that the metamaterials obtained using Ag@Si core-shell nanowires exhibit not only a negative index of refraction in the optical frequency domain, isotropic in the plane perpendicular to the nanowire axis, but, moreover, extremely low losses. f.o.m.  $\sim 200$  are achieved; about one order of magnitude better than the best reported configuration.

Since we consider a periodic arrangement of Ag@Si core-shell nanocylinders in a hexagonal lattice, a highly isotropic effective response is expected, due to the high symmetry of the unit-cell. We take the geometry of the meta-atoms to be the same as in figure 2b. For these nanostructures there is a spectral overlap between the electric and magnetic resonances for  $\lambda_0 \in (1150, 1500)$  nm. We expect a metamaterial with these basic building blocks to present a left-handed (negative-index) frequency window in which propagation is allowed. To obtain this effective response, relatively high filling fractions ( $f$ ) are expected to be needed<sup>27</sup>. Therefore, basic constituents are brought close together, fixing the surface-to-surface distance of every two neighbouring nanoparticles to be  $d_{s-s} = 10$  nm. For a hexagonal lattice this implies a filling fraction of  $f \sim 0.856$ . We have performed full numerical simulations using a Finite Element Method (FEM) commercial software (COMSOL Multiphysics 4.2). Slabs are considered infinite along transverse direction by imposing appropriate periodic boundary conditions to the system (see section Methods for further details). Let us now define a basic layer of these slabs to be such that different thicknesses are obtained by adding a different number of these layers, without need of any lateral translations. They are infinite in the transverse directions, and we call them unit constituents of the slabs (u.c.).

In Fig. 4a, the obtained transmission spectra under normal incidence illumination are depicted. Results for slabs of several

thicknesses, expressed in terms of the number of unit constituents,  $N$ , are included, the basic u.c. being described in the inset of figure 4b. A frequency window in which propagation is allowed is present, which coincides with the range in which both resonances overlap. Thus, coupling between neighbouring nanostructures does not seem to have a high impact, since the resonances are not critically modified. Recall that, although  $d_{s-s}$  is small compared to the size of the structures, the highest near field intensities are located in the surface of the core. Since core-to-core distances,  $d_{c-c}$ , are of the order of  $d_{c-c} \sim 2(R_{out} - R_{in})$ , coupling between plasmon modes is very weak, and the resonances are not disturbed. Modulations of the intensity inside the transmission window correspond to well known Fabry-Perot modes inside the slab, due to multiple reflections. The transmission peak arising at higher energies ( $\lambda \sim 1050$  nm), slightly redshifted with respect to the electric-quadrupole-like resonance, almost completely disappears for sufficiently thick slabs, as evidenced in the 60 u.c.-thick slab case (see the inset in Fig. 4a). The obtained values within the transmission frequency range decrease with the thickness of the slab due to absorption in the system. Nevertheless, there is still a significant amount of energy transmitted through, even for such a thick slab as the one with 60 u.c. (i.e. for propagation lengths inside the NIM of about 36  $\mu\text{m}$ ). Within this frequency window, negative refraction is thus expected with low associated losses. Before retrieving the values of the effective parameters, let us show that this NIM is, moreover, highly isotropic. To do so, we have performed the same study for several angles of illumination,  $\theta_i$ . Results obtained for the 60 u.c.-thick slab and  $\theta_i \in (0^\circ, 45^\circ)$  are shown in Fig. 4b. For low angles of incidence,  $\theta_i \in (0^\circ, 35^\circ)$ , transmission curves are almost identical. For increasingly higher angles of incidence,  $\theta_i \in (35^\circ, 45^\circ)$  a Fabry-Perot modulation of the transmission is observed in the high frequency limit.

**Negative refractive index retrieval.** As previously mentioned, we took three alternative approaches to determine, within the transmission window,  $Re(n_{\text{eff}})$  from simulations. The results thus obtained are depicted in the lower panel of Fig. 5. First, we have applied standard retrieval procedures<sup>28,29</sup>, which allows one to determine the effective parameters from complex reflection and transmission coefficients (or S-parameters) under normal incidence illumination, assuming an equivalent homogeneous slab. The blue dashed curve represents the obtained values. We have then applied Snell's law to those slab configurations in which the angle of incidence is  $\theta_i \neq 0$ . The results for the particular case of a 20 u.c.-thick slab under  $\theta_i = 20^\circ, 30^\circ$  illumination are plotted as red and green squares. Additionally, we simulated a rectangular prism with an angle  $\theta_{\text{prism}} = 30^\circ$  and applied Snell's law: the thus retrieved values are indicated by black circles. Both insets represent the electric field component parallel to the first interface in the slab and prism configurations for  $\lambda \sim 1215$  nm. Negative refraction with extremely low losses is clearly evident. Moreover, phase reversal, characteristic of systems having simultaneously  $\epsilon < 0$  and  $\mu < 0$ , can be observed by plotting dynamically this component in a full harmonic cycle (see Supplementary Videos 1 and 2). Errors in those values, retrieved graphically from Snell's law, have been computed by assuming a systematic error in the determination of the angle of  $\pm 2^\circ$ . It is apparent from Fig. 5 that the retrieved values are consistent regardless of the angle of incidence, indicating, as expected, that the obtained metamaterial is highly isotropic.

It is important to mention that, although the standard retrieval procedure based on S-parameters allows one to compute the index of refraction in the whole frequency range, the effective medium description of the system breaks down at longer wavelengths inside the transmission window. If somehow counter-intuitive, this effect is a consequence of the fact that  $\partial Re(n_{\text{eff}}(\omega))/\partial \omega > 0$  (non-anomalous dispersion), leading to higher absolute values at longer wavelengths, which result in shorter effective wavelengths inside the metamaterial,

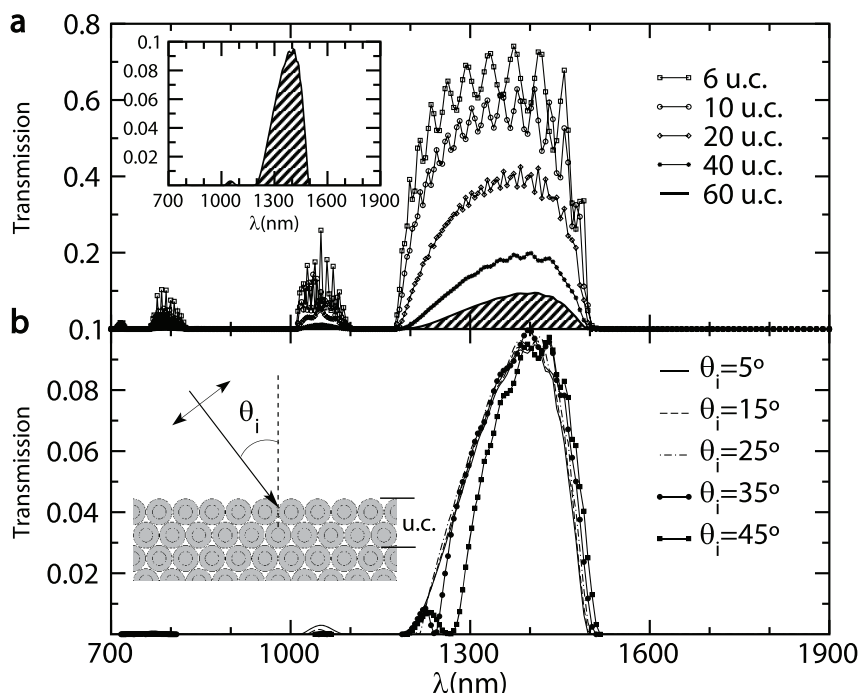


**Figure 4** | Transmission curves through metamaterial slabs made of a regular hexagonal arrangement of Ag@Si core-shell nanowire with external radius  $R_{\text{out}} = 170$  nm and internal radius  $R_{\text{int}} = 80$  nm. Centre-to-centre distance between neighbours is  $L = 350$  nm. (a) Transmission curves for several thicknesses under normal incidence illumination, corresponding to different symbols. The inset shows the case of a slab with a thickness of 60 unit constituents (u.c.). (b) Transmission curves through a 60 u.c.-thick slab under several angles of incidence.

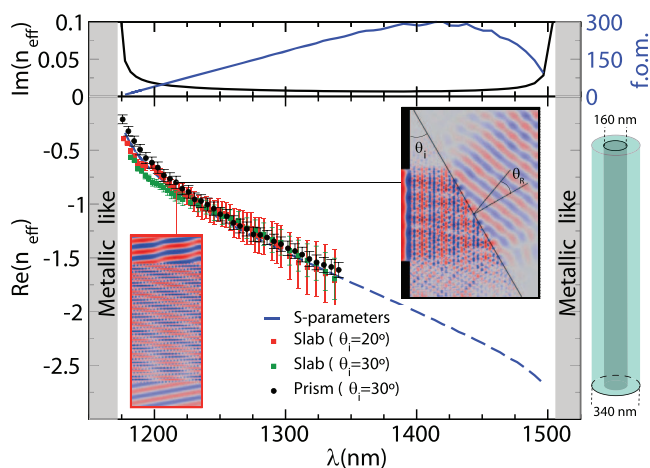


**Figure 5** | Effective index of refraction of a metamaterial built with Ag@Si core-shell nanowires with  $R_{\text{int}} = 80$  nm and  $R_{\text{out}} = 170$  nm arranged in a hexagonal lattice. Lower Panel: Retrieved real part of the index of refraction. The blue discontinuous curve represents the values obtained from complex reflection and transmission coefficients under normal incidence. Black circles represent the retrieved values from Snell's law in the prism configuration. The incidence angle is fixed,  $\theta_i = \theta_{\text{prism}} = 30^\circ$ . The corresponding inset shows the y-component of the electric field (only non-zero of the incident wave) for the particular case  $\lambda \sim 1215$  nm. Red and green squares represent the values obtained from Snell's law in the slab configuration. Angles of incidence are  $\theta_i = 20^\circ$  (red) and  $\theta_i = 30^\circ$  (green). The corresponding inset represents the x-component (parallel to the first interface) of the electric field for  $\lambda \sim 1215$  nm. Error bars computed assuming a systematic error in the determination of the refracted angle of  $\pm 2^\circ$ . Upper Panel: Imaginary part of the index of refraction obtained from complex reflection and transmission coefficients (black curve) and the corresponding figure of merit, f.o.m., as defined in the text (blue curve).

$\lambda_{\text{eff}}$ . In this way, at  $\lambda_0 = 1150$  nm, the effective wavelength inside the structure can reach  $\lambda_{\text{eff}} = \lambda_0 / |Re(n_{\text{eff}})| \sim 15 \mu\text{m}$ , i.e., up to 40 times the characteristic period length within the structure. By contrast, at  $\lambda_0 = 1500$  nm,  $\lambda_{\text{eff}} = \lambda_0 / |Re(n_{\text{eff}})| \sim 575$  nm, so that the effective wavelength inside the system is smaller than two times the period. Therefore, when the retrieved refractive index becomes very large (despite being negative), the effective wavelength inside the metamaterial becomes correspondingly small, thus becoming of the order of the lattice constant. At such limit, we do not fully trust the resulting refractive index, at least from the point of view of proper NIM behavior, thus establishing a cutoff in Fig. 4.

**Losses and Figure of merit.** With respect to losses, there is a strong evidence that the metamaterial is very weakly absorbing, as deduced from the fact that the transmission values are as high as 0.1 within the negative-index band, with about the same portion of reflection, for propagation lengths inside the metamaterial of about  $36 \mu\text{m}$ . This extremely low attenuation of waves propagating inside the NIM is also evident in the electric near field maps (see insets in figure 5). One can actually compute the expected values of the imaginary part of the index through the standard S-parameter retrieval procedure: The results are plotted in the upper panel of figure 5. While values as extraordinarily low as  $7 \times 10^{-3}$  are achieved within the transmission window, out of it, the metamaterial essentially behaves as a metal, with  $Re(n_{\text{eff}}) < Im(n_{\text{eff}})$ , reflecting almost entirely the incident wave. Inside the negative-index band, values of the figure of merit (f.o.m. =  $-Re(n_{\text{eff}})/Im(n_{\text{eff}})$ ) can, in turn, be as high as f.o.m.  $\sim 200$ . In the particular case of  $Re(n_{\text{eff}}) = -1$ , f.o.m.  $\sim 85$ , i.e.,  $Im(n_{\text{eff}}) = 0.012$ . Recall that the f.o.m. in the case of core-shell nanospheres is substantially lower<sup>27</sup>, stemming from their much larger absorption efficiency, as compared to that of core-shell cylinders.

To further test the validity of this proposal, similar analysis has been performed to the case of Ag@Ge core-shell nanowires arranged, instead, in a square lattice (keeping the  $d_{s-s}$  constant). Results indicate that the so obtained metamaterial behaves as a NIM in the



$\lambda_0 \in (1.3, 1.45) \mu\text{m}$  frequency range. Values for the real part of the index are slightly lower and associated losses higher (see Section 2 in the Supplementary Information). Concerning the metal core, any other metal with a good ‘plasmonic’ behavior can be used, like Au or Cu, leading indeed to a quite similar low-loss NIM behavior.

## Discussion

As showed here, metallo-dielectric core-shell nanowires of circular cross section, are very promising candidates as building blocks of highly isotropic, negative index metamaterials operating at optical frequencies, with extremely low losses exhibiting figures of merit f.o.m.  $\sim 200$  (an order of magnitude larger than previously proposed NIMs). Although here demonstrated to operate at  $\lambda_0 \in (1.15, 1.35) \mu\text{m}$  for Ag@Si with  $R_{\text{int}} = 80 \text{ nm}$  and  $R_{\text{out}} = 170 \text{ nm}$  arranged in a hexagonal lattice, and at  $\lambda_0 \in (1.3, 1.45) \mu\text{m}$  for Ag@Ge nanowires with  $R_{\text{int}} = 90 \text{ nm}$  and  $R_{\text{out}} = 170 \text{ nm}$  arranged in a square lattice, negative refraction in the whole telecom frequency range can be achieved by tuning the geometrical parameters. We have also verified that the low-loss NIM behavior can be scaled down to 800 nm by introducing a thin layer of a low index material (i.e. silica) in between the Ag core and the Si shell. Theoretically, such thin layer would produce a slight blueshift of the dipolar electric resonance; correspondingly, the magnetic resonance could be properly matched by tuning the shell dimensions. To further downscale the design into the visible, a nearly lossless semiconductor should be employed. Moreover, the operating physical principles can be applied to obtain negative refraction in completely different ranges of the electromagnetic spectrum (IR and THz) by using appropriate materials.

We also anticipate that the proposed design, though challenging, is no doubt amenable to fabrication at present. For instance, nanoporous silicon templates can be easily fabricated in arrays with long-range order in various manners<sup>31,32</sup>; indeed, core-shell Si NWs<sup>33</sup> or even hollow Si nanowires<sup>34</sup> have been very recently obtained with suitable dimensions. For our proposed NIM design, filling those holes with Ag or Au would then suffice. Recall that many other high-index, nearly lossless semiconductors exist that will lead to the same NIM behavior. In this regard, for instance, hollow AlInP semiconducting nanowires have been patterned by metal-organic vapor phase epitaxy in a photoresist matrix<sup>35</sup>, filling the hollows with a noble metal prior to photoresist removal would complete the process. On the other hand, it should be mentioned that, if needed for fabrication purposes, a thin shell of silica (or any other low-index dielectric, as mentioned above) could be deposited as an intermediate layer between the noble metal and the semiconductor shell.

In addition, semiconducting core-shell nanowires have been fabricated by a two-step growth process combining selective-area and vapor-liquid-solid epitaxy<sup>35</sup>. Furthermore, we anticipate the robustness of the proposed design against NW size inhomogeneities and array defects/disorder; this stems from the broad spectral width of the NW resonances and resulting negative-index bands, along with the fact that the latter does not critically depend on the NW particular arrangement.

## Methods

The scattering properties of solid and core-shell cylinders were computed analytically following references<sup>26,30</sup> (see also Supplementary Information, Section 1).

Corresponding near field maps were also computed analytically with this formalism.

Full electromagnetic simulations of propagation of waves inside slabs and prisms were carried out using a Finite Element Method commercial software (COMSOL Multiphysics 4.2). In the case of slabs, Bloch boundary conditions are applied at the lateral ends of the simulation domain to reproduce an infinite system. At the boundaries ahead and behind the slab, complex transmission and reflection coefficients (S-parameters) are computed. We use the built-in port boundary condition to this end. The effective material parameters are, then, retrieved from the S-parameters according to<sup>27,29</sup>. Although the imaginary part of the effective index quickly converges with increasing number of functional layers, retrieval of the real part implies an ambiguity in the election of the branch of the complex logarithm<sup>29</sup>. To get rid of such ambiguity several slab thicknesses were simulated. In particular, we simulated slabs made of 2, 3, 4, 5, 6, 7, 10, 20, 30, 40 and 60 functional layers (not all shown in figure 4).

Silicon was assumed lossless in the frequency range studied, with a refractive index of  $n_{\text{Si}} = 3.5$ . Nonetheless, to make sure that the small imaginary part of Si is not affecting the resulting f.o.m., numerical calculations including it were carried out, yielding the same f.o.m. See Supplementary Information for a comparison of the optical properties of core-shell nanowires when losses are taken into account, as well as the retrieved imaginary part and figure of merit. Silver material properties were taken from experimental values from reference<sup>36</sup>.

- Ramakrishna, S. A. Physics of negative refractive index materials. *Rep. Prog. Phys.* **68**, 449–521 (2005).
- Marques, R., Martin, F. & Sorolla, M. *Metamaterials with Negative Parameters: Theory, Design and Microwave Applications* (Wiley, 2007).
- Pendry, J. B. Negative refraction makes a perfect lens. *Phys. Rev. Lett.* **85**, 3966–3969 (2000).
- Zhang, X. & Liu, Z. Superlenses to overcome the diffraction limit. *Nature Mater.* **7**, 435–441 (2008).
- Jacob, Z., Smolyaninov, I. I. & Narimanov, E. E. Broadband Purcell effect: Radiative decay engineering with metamaterials. *Appl. Phys. Lett.* **100**, 181105 (2012).
- Pendry, J. B., Schurig, D. & Smith, D. R. Controlling Electromagnetic Fields. *Science* **312**, 1780–1782 (2006).
- Leonhardt, U. Optical Conformal Mapping. *Science* **312**, 1777–1780 (2006).
- Soukoulis, C. M. & Wegener, M. Past achievements and future challenges in the development of three-dimensional photonic metamaterials. *Nature Photon.* **5**, 523–530 (2011).
- Shalaev, V. M. Optical negative-index metamaterials. *Nature Photon.* **1**, 41–48 (2007).
- Zhou, J. *et al.* Saturation of the magnetic response of split-ring resonators at optical frequencies. *Phys. Rev. Lett.* **95**, 223902 (2005).
- Burgos, S. P., de Waele, R., Polman, A. & Atwater, H. A. A single-layer wide-angle negative-index metamaterial at visible frequencies. *Nature Mater.* **9**, 407–412 (2010).
- Yao, J. *et al.* Optical Negative Refraction in Bulk Metamaterials of Nanowires. *Science* **321**, 930–930 (2008).
- Alú, A., Salandrino, A. & Engheta, N. Negative effective permeability and left-handed materials at optical frequencies. *Opt. Express* **14**, 1557–1567 (2006).
- O’Brien, S. & Pendry, J. B. Photonic band-gap effects and magnetic activity in dielectric composites. *J. Phys.: Condens. Matter* **14**, 4035–4044 (2002).
- Jelinek, L. & Marqués, R. Artificial magnetism and left-handed media from dielectric rings and rods. *J. Phys.: Condens. Matter* **22**, 025902 (2010).
- Wheeler, M. S., Aitchison, J. S. & Mojahedi, M. Three-dimensional array of dielectric spheres with an isotropic negative permeability at infrared frequencies. *Phys. Rev. B* **72**, 193103 (2005).
- Popa, B. I. & Cummer, S. A. Compact dielectric particles as a building block for low-loss magnetic metamaterials. *Phys. Rev. Lett.* **100**, 207401 (2008).
- García-Etxarri, A. *et al.* Strong magnetic response of submicron Silicon particles in the infrared. *Opt. Express* **19**, 4815–4826 (2011).
- Zhao, Q., Zhou, J., Zhang, F. & Lippens, D. Mie resonance-based dielectric metamaterials. *Mat. Today* **12**, 60–69 (2009).
- Vynck, K. *et al.* All-dielectric rod-type metamaterials at optical frequencies. *Phys. Rev. Lett.* **102**, 133901 (2009).
- Schuller, J. A., Zia, R., Taubner, T. & Brongersma, M. L. Dielectric metamaterials based on electric & magnetic resonances of silicon carbide particles. *Phys. Rev. Lett.* **99**, 107401 (2007).
- Valentine, J. *et al.* Three-dimensional optical metamaterial with a negative refractive index. *Nature* **455**, 376–379 (2008).
- Zhang, S. *et al.* Optical negative-index bulk metamaterials consisting of 2D perforated metal-dielectric stacks. *Opt. Express* **14**, 6778–6787 (2006).
- Zhou, J., Koschny, T., Kafesaki, M. & Soukoulis, C. M. Negative refractive index response of weakly and strongly coupled optical metamaterials. *Phys. Rev. B* **80**, 035109 (2009).
- Kuester, E. F. *et al.* A negative refractive index metamaterial based on a cubic array of layered nonmagnetic spherical particles. *Progress In Electromagnetics Research B* **33**, 175–202 (2011).
- Kerker, M. & Matijević, E. Scattering of electromagnetic waves from concentric infinite cylinders. *J. Opt. Soc. Am.* **51**, 506–508 (1961).
- Paniagua-Domínguez, R., López-Tejeda, F., Marqués, R. & Sánchez-Gil, J. A. Metallo-dielectric core-shell nanospheres as building blocks for optical three-dimensional isotropic negative-index metamaterials. *New J. Phys.* **13**, 123017 (2011).
- Smith, D. R., Vier, D. C., Koschny, T. & Soukoulis, C. M. Electromagnetic parameter retrieval from inhomogeneous metamaterials. *Phys. Rev. E* **71**, 036617 (2005).
- Chen, X., Grzegorzczak, T. M., Wu, B., Pacheco, J. Jr. & Kong, J. A. Robust method to retrieve the constitutive effective parameters of metamaterials. *Phys. Rev. E* **70**, 016608 (2004).
- Bohren, C. F. & Huffman, D. R. *Absorption and Scattering of Light by Small Particles* (Wiley, 1983).
- Xia, D., Ku, Z., Lee, S. C. & Brueck, S. R. J. Nanostructures and functional materials fabricated by interferometric lithography. *Adv. Materials* **23**, 147–179 (2011).



32. Zhang, Z., Zou, R., Yu, L. & Hu, J. Recent Research on One-Dimensional Silicon-Based Semiconductor Nanomaterials: Synthesis, Structures, Properties and Applications. *Critical Reviews in Solid State and Materials Sciences* **36**, 148–173 (2011).
33. Zhou, Y., Liu, Y., Cheng, J. & Lo, Y. Bias dependence of sub-bandgap light detection for coreshell silicon nanowires. *Nano Lett.* **12**, 5929–5935 (2012).
34. Algra, R. E. *et al.* Crystal structure transfer in core/shell nanowires. *Nano Lett.* **11**, 1690–1694 (2011).
35. Sköld, N. *et al.* Nanofluidics in hollow nanowires. *Nanotechnology* **21**, 155301 (2010).
36. Johnson, P. B. & Christy, R. W. Optical constants of the noble metals. *Phys. Rev. B* **6**, 4370 (1972).

## Acknowledgements

The authors acknowledge M. Nieto-Vesperinas and R. Marqués for fruitful discussion in the preparation of this manuscript. They also acknowledge the Spain Ministerio de Economía y Competitividad, through the Consolider-Ingenio project EMET (CSD2008-00066) and NANOPLAS+ (FIS2012-31070), and the Comunidad de Madrid (grant MICROSERES P2009/TIC-1476) for support. R. P.-D. also acknowledges support from The European Social Fund and CSIC through a JAE-Pre grant.

## Authors contributions

R.P.D. and J.A.S.G. conceived the idea and designed the theoretical framework. D.R.A. conducted the Mie scattering calculations. R.P.D. conducted the numerical simulations and wrote the main manuscript text. J.A.S.G. supervised the research. All authors discussed the results and reviewed the manuscript.

## Additional information

**Supplementary information** accompanies this paper at <http://www.nature.com/scientificreports>

**Competing financial interests:** The authors declare no competing financial interests.

**License:** This work is licensed under a Creative Commons Attribution-NonCommercial-NoDerivs 3.0 Unported License. To view a copy of this license, visit <http://creativecommons.org/licenses/by-nc-nd/3.0/>

**How to cite this article:** Paniagua-Domínguez, R., Abujetas, D.R. & Sánchez-Gil, J.A. Ultra low-loss, isotropic optical negative-index metamaterial based on hybrid metal-semiconductor nanowires. *Sci. Rep.* **3**, 1507; DOI:10.1038/srep01507 (2013).